Engineering Solutions to Mechanics, Marine Structures and Infrastructures

Eng. Solut. Mech. Mar. Struct. Infrastruct.
2024.1(2).7
ISSN：2960-0979
https://doi.org/10.58531/esmmsi/1/2/7

Article

The Effect of the Support Mass in 3D Printing on the Forming Time of the Model

Zhenjie Liang[1], Yifan Xie[1], Yining Zhang[1],Guanyixuan Zhao[1],Qifeng Lin[1],Dapeng Zhang[1,*],Haoyu Jiang[2]

[,1] Ship and Maritime College, Guangdong Ocean University, Zhanjiang 524005 China
[2] School of Electronics and Information Engineering, Guangdong Ocean University, Zhanjiang 316021, China

Academic Editor: Weiwei Wang < zhwangww@ytu.edu.cn>

Received: 1 May 2024; Revised: 12 May 2024; Accepted: 17 May 2024; Published: 17 May 2024

Abstract: 3D printing technology has a very wide range of applications in various fields, when rapid manufacturing and chain stability are required in production; 3D printing technology can fulfil both conditions. However, limited by printer specifications, medium to large components must be printed in sections. For the quality of the products it is sometimes necessary to adjust the angle of placement of the model, these will affect the time it takes to print the model. This paper will investigate the intricate interplay between support mass and printing time, tilt angle and support mass, as well as tilt angle and forming time, utilizing two distinct 3D printing technologies: FDM and UV-Curing. Furthermore, we aim to compile comprehensive data Tables and line graphs to provide a visual representation of our findings. This paper can provide insights into the further development of 3D printing for the manufacture of medium to large parts and promote their wider application and research in various fields.

Keywords: 3D printing; Angle of placement; Support mass

Citation: Liang Z., Xie Y., Zhang Y., Zhao G., Lin Q., Zhang D., Jiang H. The Effect of the Support Mass in 3D Printing on the Forming Time of the Model. Eng. Solut. Mech. Mar. Struct. Infrastruct., 2024, 1(2), doi: 10.58531/esmmsi/1/2/7

1. Introduction

With the development of technology and economy, industrial products are not only a necessity for people, but also play a very important role in maintaining the stability of the society and even the country. Therefore, the stability of the production of industrial products is particularly important, and the emergence of 3D printing technology has brought a better solution to this problem. Traditional manufacturing produces products by cutting, trimming, thwarting, and other material reduction methods, this process will generates a lot of material waste; moreover, the production process sometimes generates a large amount of dust, which enters the lungs by the respiratory tract and causes some damage to the human body. Human-dependent manufacturing is highly susceptible to biological factors, such as the COVID-19; which leads to instability in the production chain. And 3D printing technology is also called additive manufacturing [1], The final product is obtained by layering materials on top of each other; this process greatly reduces material wastage and ensures the stability of the production chain. 3D printing technology has a wide range of applications in architecture, aerospace, biomedicine and many other fields, printing materials such as metals, ceramics, photosensitive resins, food materials and so on [2]. Contributed greatly to the field of materials research in the field of shipbuilding and research on offshore structures. [3-5] . The Oak Ridge National Laboratory's Manufacturing Demonstration Facility and the U.S. Navy's Destructive Technology Laboratory collaborated on the first military-printed 3D submarine shell [6] in 2017. The oceans, as the vast expanse of the earth, are rich in resources waiting to be exploited; the construction of ships and offshore platforms is necessary for the exploration of the oceans [7].Due to the limitations of current technology, the maximum space that can be moulded by today's 3D printers is a square with a side length of 12m. Meng lei Mei, Qi Qin and others segment printing method proposed to provide ideas for large ship construction, they were also used the software to investigate the relationship between the amount of support added to the hull of a segmentally printed ship and the printing time [8]. With reference to this research methodology, this paper will delve deeper into the effect of multiple variables on printing time by controlling variables and increasing or decreasing the support mass by changing the angle of the model's placement, we propose some suggestions and reference methods for the future 3D printing of producting medium and large components, ship models and other fields.

2. Software and 3D Printers Will be Needed.

2.1 Modelling Software: Solidworks;3ds Max

Both types of software are used to build 3D models, and both types of them have their advantages and disadvantages. 3ds Max is easier and simpler than solidworks for surface design. Solidworks [9, 10] has a great advantage in parts, mechanical design, parts assembly, the software can easily use multiple custom planes to split the 3D model into multiple parts, so we will use 3ds Max [11] to model the model and solidworks to split it. STL format is the

common "language" of slicing software and 3D modelling software [12], 3ds Max builds the model and then exports it to STL format and then uses solidworks to import it.

2.2 Slicing Software: Bambu Studio ;CHITUBOX

The principle of slicing software is to convert a digital 3D model into a code can be recognised by the 3D printer and then execute that code on the 3D printer. Generally speaking, different slicing software corresponds to different types of 3D printers, but some of them are common, Bambu Studio for FDM printers, CHITUBOX for light-curing printers.

2.2.1 Fused Deposition 3D Printer (FDM)

FDM, was also named Fused Filament Fabrication (FFF), is an additive manufacturing process that belongs to the material extrusion series [13]. During operation, thermoplastic materials [14], including acrylonitrile-butadiene-styrene terpolymer (ABS), polylactic acid (PLA), polycarbonate (PC), and others, are heated to a melting temperature within the nozzle of the Fused Deposition Modeling (FDM) printer. Under the influence of gravity, the melted thermoplastic gracefully drips from the nozzle, landing precisely on the print bed. Guided by the slicing software, the nozzle traces a preplanned three-dimensional path, following the code until the print is flawlessly completed.

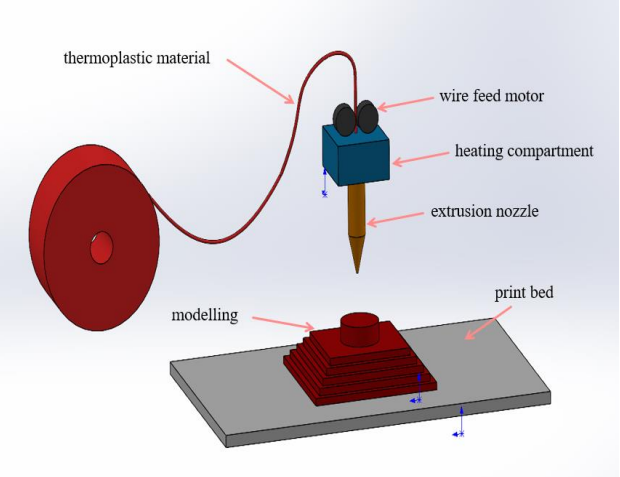

Figure. 1.FDM working sketch

2.2.2 Light-Curing 3D Printers (UV-Curing 3D Printing)

The core principle of light-curing 3D printing [15] technology lies in the selective curing of photosensitive resin [16], encompassing high-temperature-resistant resins like H100, ABS high-strength resins such as A200 eResin-ABS Pro, and versatile rigid resins known as Standard Resin. This curing process is achieved through the application of ultraviolet light, precisely controlled by digital signals. The cured resin builds up layer by layer until a complete model is formed, photosensitive resins have become the material of choice for 3D printing of high-precision products due to their excellent fluidity and instantaneous light-curing properties [17].

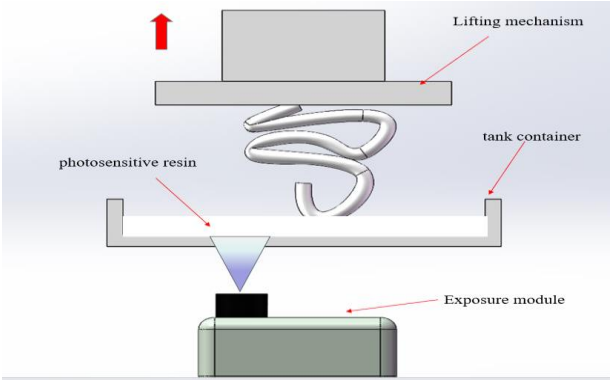

Figure. 2. Light-curing 3D printers working sketch

3. Build and Segment Models

This article will model part of the hull for research purposes, only the hull shell and part of the superstructure will be modelled. Firstly, we use 3ds Max to build the overall model, and then use solidworks to divided it into A, B, C three parts; divided out of each part are saved as a separate file (STL format). We import the file into the slicing software [18] and we can zoom in and out of the model, change the material, add supports and other parameters that you want to change in the model. Once the model has been processed in the slicing software, the file can be loaded into the 3D printer to begin the printing process.

Currently, there exists a plethora of industrial design software capable of meeting a wide range of design needs. However, the transition from modeling to configuring various parameters in slicing software is currently a manual process. If artificial intelligence were to be employed to seamlessly integrate these three processes—modeling, slicing, and printing—leaving humans only to articulate their requirements, it would undoubtedly signify a significant advancement for the manufacturing industry. This endeavor necessitates extensive employment of machine learning techniques like Physical Information Neural Networks (PINNs) [19] and the accumulation of substantial experimental data. For instance, understanding the fluid properties of thermoplastic materials as they melt or the physical effects of the flow of photosensitive resin during the light curing process. These challenges call for expertise in fluid mechanics [20,21], including Computational Fluid Dynamics.

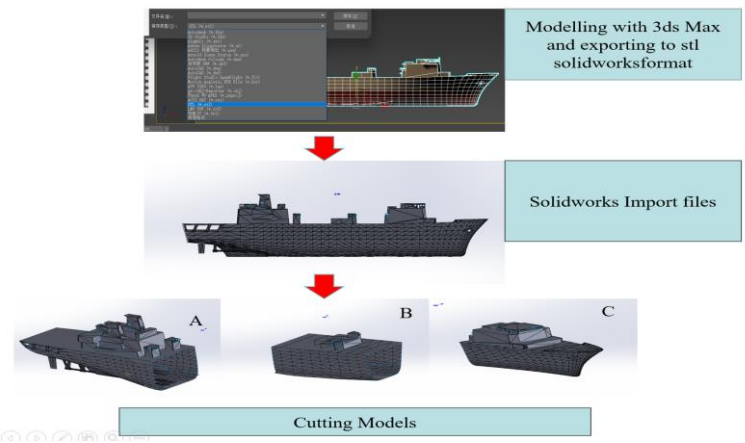

Figure. 3. Modelling and cutting

4. Relevant Size Data

Table 1. Representation of physical quantities.

Letters used to represent	Meaning
V	volume
M	Mass
T	Time
K	Percentage of reduction and magnification
θ	Tilt Angle
L	Length

The physical quantities indicated in Table 1 above, as illustrated in Fig. 3, utilize L(0)max, W(0)max, and H(0)max to represent the dimensions of the model at its longest, widest, and highest points when uncut, respectively. V(0) denotes the overall volume of the model. Additionally, L(A)max, W(A)max, H(A)max, and V(A) represent the corresponding dimensions of part A, while L(B)max, W(B)max, H(B)max, and V(B) are used for part B, and L(C)max, W(C)max, H(C)max, and V(C) for part C.

$$e + n = 10^n \tag{1}$$

Where n is a natural number, the numerical value on the right-hand side of the equation is 108 for n = 8.

4.1 Original Dimensional Parameters of Each Model

L(0)max =178499 mm, W(0)max =25284.5 mm, H(0)max =32026.4 mm, V(0)=5.71265(e+13) mm3.

Part A：

$L(A)_{max}$ =71862 mm, $W(A)_{max}$ =24800.3mm, $H(A)_{max}$ =32026.4 mm, V(A)=2.43991(e+13) mm^3.

Part B：

$L(B)_{max}$=44243.9 mm, $W(B)_{max}$ =25285.5mm, $H(B)_{max}$ =22227.2 mm, V(B)=1.81837(e+13) mm^3.

Part C：

$L(C)_{max}$ =62428.1 mm, $W(C)_{max}$ =24437 mm, $H(C)_{max}$ =28476.7 mm, V(C)=1.46692(e+13) mm^3.

The above data are shown in Table 2 below:

Table 2. Raw and dissected model data.

	L_{max}	W_{max}	H_{max}	V
Raw model	178499 mm	25284.5 mm	32026.4 mm	5.71265(e+13)mm^3
Part A	71862 mm	24800.3mm	32026.4 mm	2.43991(e+13)mm^3
Part B	44243.9 mm	25285.5mm	22227.2 mm	1.81837(e+13)mm^3
Part C	62428.1 mm	24437 mm	28476.7 mm	1.46692(e+13)mm^3

Selecting K=1/800, the reduced parameter sizes are shown in Table 3 below:

Table 3. K=1/800 model data.

	L_{max}	W_{max}	H_{max}	V
Raw model	223.12375 mm	31.6056 mm	40.033 mm	111575 mm^3
Part A	89.8275 mm	31.0004 mm	40.033 mm	47654.6 mm^3
Part B	55.3049 mm	31.6069 mm	27.784 mm	35515.1 mm^3
Part C	78.0351 mm	30.5462 mm	35.5959 mm	28650.8 mm^3

4.2 Analysis the Difference

4.2.1 When K=1

$$L(A)_{max}+L(B)_{max}+L(C)_{max}=178534\ mm>L(0)_{max}=178499\ mm \quad (2)$$

Difference: $\Delta L = 35$ mm compared to the original model.

$$V(A)+V(B)+V(C)=5.7252\ (e+13)\ mm^3> V(0)=5.71265(e+13)\ mm^3 \quad (3)$$

Volume difference: $\Delta V = 0.01255(e+13)\ mm^3$

Theoretically, the sum of the lengths of parts A, B, and C should match the original model's dimensions, and their combined volume should also be equal. However, currently, the combined length of parts A, B, and C exceeds the original model's length by 35mm, and their combined volume surpasses the original model's by 0.01255e+13 (mm^3). This translates to an approximate length error rate of 0.0196 per cent and a volume error rate of about 0.2197 per cent.

4.2.2 After Shrinking 800 Times

$$L(A)_{max}+L(B)_{max}+L(C)_{max}=223.1675\ mm> L(0)_{max}=223.12375\ mm \quad (4)$$

Difference: $\Delta L=0.04375$ mm

$$V(A)+V(B)+V(C)=111820.5\ mm^3> V(0)=111575\ mm^3 \quad (5)$$

Volume difference: $\Delta V=245.5$ mm3, the length error rate is 0.0196 per cent and the volume error rate is about 0.22 per cent.

4.2.3 STL Format Mechanism

The STL format [22-24] stores part information by creating numerous triangular facets on its surface, with the accuracy of the model determined by the quantity of these facets. However, varying software applications can produce different numbers of facets when

converting the same part to STL, even with identical settings. In this experiment, models A, B, and C are derived from the original and saved separately in STL format. A comparison reveals deviations in the number of facets and other parameters compared to the original, resulting in errors in length and volume. We find that there are deviations in the number of triangular facets and other parameters for a given tilt angle, but the difference in printing time is not significant; so we can ignore these effects.

5. Relationship Between the Amount of Added Support and the Forming Time of the Model (FDM)

5.1 Change the Angle of Model Placement

A model with more overhangs needs support before it can be printed [25,26]. The greater the number of overhangs, the more support is required. By adjusting the angle of the model in the slicing software, it's possible to alter the extent of overhangs and consequently, the amount of support needed. The mass of the support can be calculated by subtracting the mass of the unsupported model from the total mass of the model with added support. This mass measurement is used to determine the volume of support required.

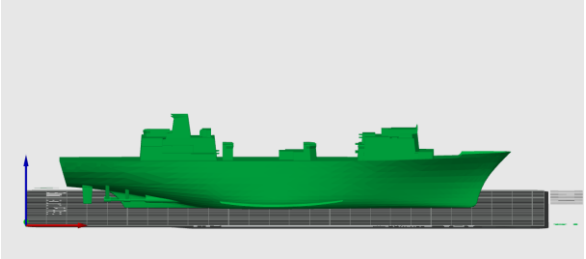

Figure. 4. Models with a tilt angle of 0°

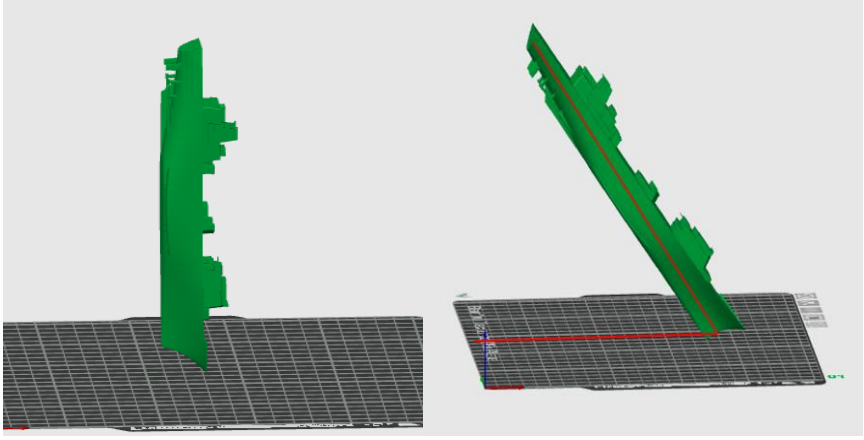

Figure. 5. Models with a tilt angle of 90°

Figure. 6. Models with a tilt angle of θ

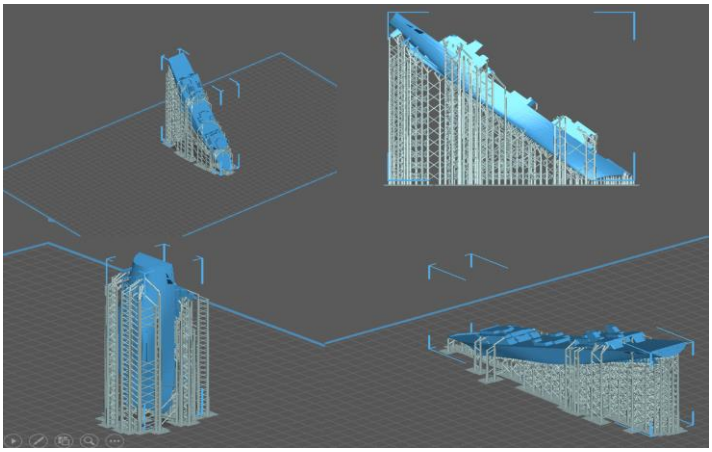

Figure. 7. Models and Support Sections

5.2 Experiments and Statistics

As shown in Figure 7, the blue part is the model part and the white part is the support part. As shown in Fig. 4, the model is placed squarely, and the mass of the model is 43.33g (the printing material is PLA) and the mass of the support is 0g; the time needed for forming the model is 87 minutes. Place the model as shown in Fig. 5, where the total mass is 59.32g and the supporting mass is 15.99g; the time taken to form the model is 201 minutes. The model is positioned at an angle to the printing plate as illustrated in Fig. 6, with the angle marked as the angle between the two red lines in the Figure, denoted as θ. The mass of the model, the mass of the support, and the time required for forming the model with different values are provided in the Table 4 below:

Table 4. K=1/800 model data.

θ	Total mass (g)	Mass of the support (g)	T (min)
0°	43.33	0	87
10°	69.24	25.91	182
12°	73.92	30.59	201
15°	78.60	35.27	222
18°	78.01	34.68	188
20°	79.13	35.8	186
25°	83.89	40.46	203
28°	82.77	39.44	209
30°	83.74	40.41	216
35°	50.37	7.04	159
45°	50.34	7.01	164
60°	54.83	11.5	187
75°	58.02	14.69	210
80°	59.56	16.23	211
90°	59.32	15.99	207

5.3 Plotting and Analysing Line Graphs

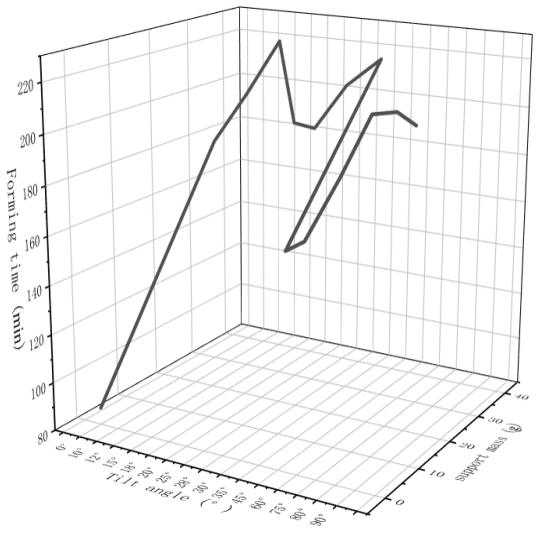

Figure. 8. Relationship between tilt angle support mass and forming time

Figure 8 illustrates the intricate interplay among forming time, tilt angle, and support mass. The relationship depicted bears resemblance to a segmented function. Initially, within the tilt angle range of θ = (0°, 15°), there is a discernible positive correlation between moulding time and support mass. As the tilt angle extends to θ = (15°, 35°), the relationship becomes more complex, manifesting fluctuation akin to wave-like patterns albeit with relatively minor amplitudes. Moreover, within the range of θ = (35°, 80°), a positive correlation between the three variables reemerges. However, beyond this interval, the correlation shifts towards negativity.

Viewed from a macroscopic standpoint, no overarching pattern emerges across the relationships; rather, significance is observed only within specific intervals. This phenomenon suggests the presence of other potential coupling factors [27] that exert influence on the dynamic interrelationship among these three variables.

5.4 Separate Printing (FDM)

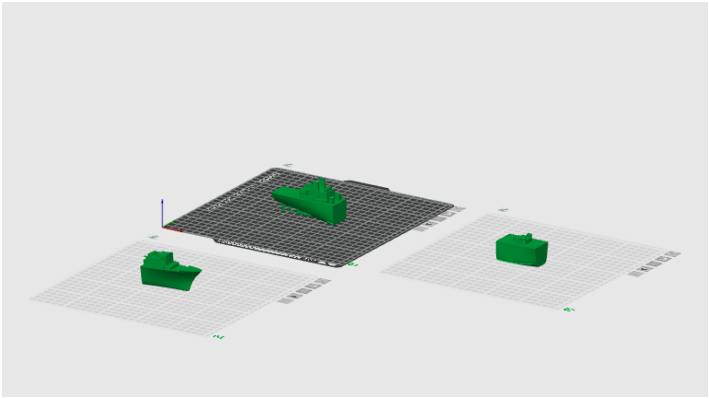

Figure. 9. Parts A, B and C

As depicted in Figure 9, parts A, B, and C are positioned squarely in the print tray, without the addition of any support or rotation (θ = 0°). The quality and printing time of each part are detailed in Table 5:

Table 5. K=1/800 model A, B and C data.

Model parts	M	Printing time
A	19.67 g	52 min
B	13.05 g	31 min
C	12.23 g	36 min

The combined mass of the three parts is 44.95g, which is 1.62g more than that of the original model. Additionally, the printing time for these parts totals 119 minutes, indicating an increase of 32 minutes compared to the original model. Consequently, segment printing results in a 40% increase in printing time compared to printing the original model as a whole. Whether to opt for segmented printing should be determined by specific circumstances. For instance, if the printed model surpasses the printer's capacity or if additional parts such as electronic components need to be incorporated into a section of the finalized model.

The data in part A are shown in the Figure10 and Table 6 below:

Table 6. Data Tables for part A.

θ (°)	Support mass (g)	Printing time (min)
0	0	52
10	8.32	92
12	9.35	99
15	10.38	106
18	8.05	85
20	8.51	87
25	8.41	90
28	6.23	85
30	6.44	87
35	1.61	77
45	2.83	84
60	6.84	97
75	5.62	98
80	4.82	96
90	2.51	87

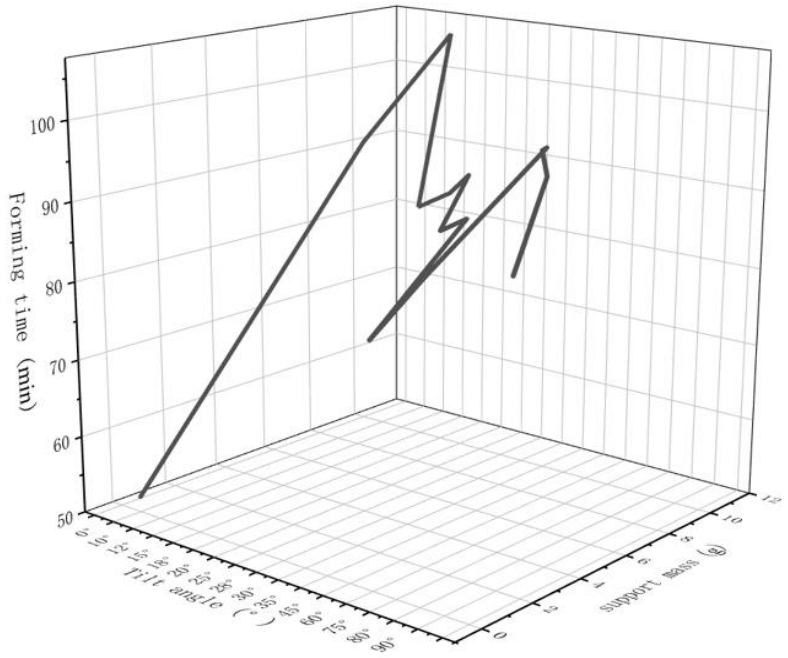

Figure. 10. Line graph of the three relationships in part A

The data in part B are shown in the Figure 11 and Table 7 below:

Table 7. Data Tables for part B.

θ (°)	**Support mass (g)**	**Printing time (min)**
0	0	31
10	4.02	48
12	5.06	53
15	5.72	58
18	5.02	47
20	5.4	48
25	6.23	51
28	6.89	57
30	6.84	58
35	1.36	45
45	1.34	46
60	2.01	51
75	2.00	54
80	1.52	51
90	0.74	46

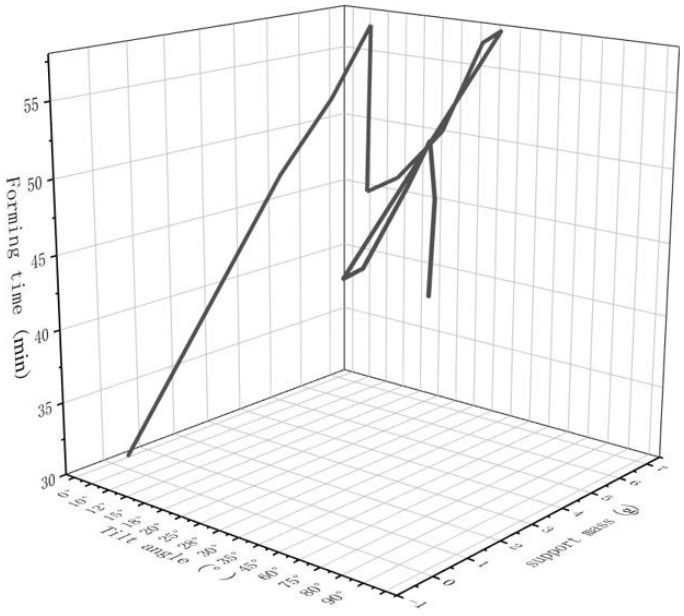

Figure. 11. Line graph of the three relationships in part B

The data in part C are shown in the Figure 12 and Table 8 below:

Table 8. Data Tables for part C.

θ (°)	**Support mass (g)**	**Printing time (min)**
0	0	36
10	4.41	58
12	4.93	56
15	2.15	45
18	5.34	62
20	4.78	56
25	4.92	57
28	5.39	59
30	5.57	61
35	1.63	54
45	1.53	56
60	1.58	55
75	3.95	67
80	3.78	66
90	4.86	68

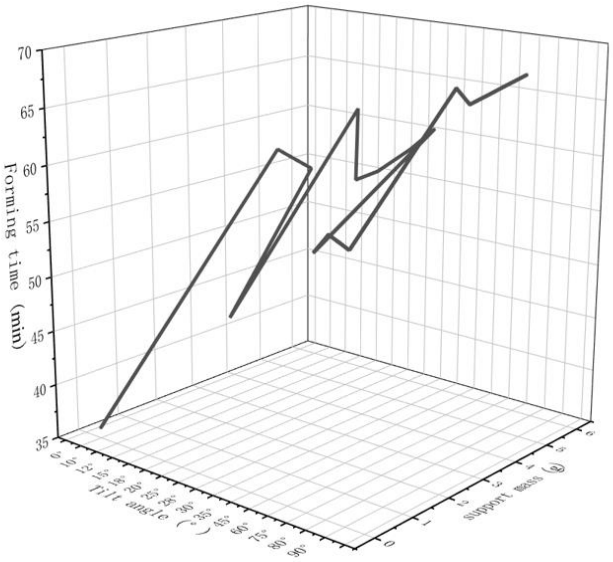

Figure. 12. Line graph of the three relationships in part C

After careful statistics and analyses, we collected the data on the support mass and forming time of the original model, Model A, Model B and Model C at multiple inclination angles, and drew 3D line graphs for these data respectively. After carefully observing Figures 8, 10, 11 and 12, it is not difficult to find that the four fold lines in these plots show similarity in the same inclination angle intervals, with similar patterns of change and trends. This finding provides a strong data support for our in-depth understanding of the performance of each model under different inclination angles.

After thoroughly analyzing the data within these four Tables and conducting a comprehensive comparison of the trends depicted in each Table, a preliminary assumption can be made suggesting a positive correlation between support mass and molding time, provided the inclination angle remains constant. However, it is important to note that the presence of occasional outliers in the dataset deviating from this pattern prevents us from conclusively asserting a completely positive relationship between the two variables.

5.4.1 Set the Tilt Angle = 90°

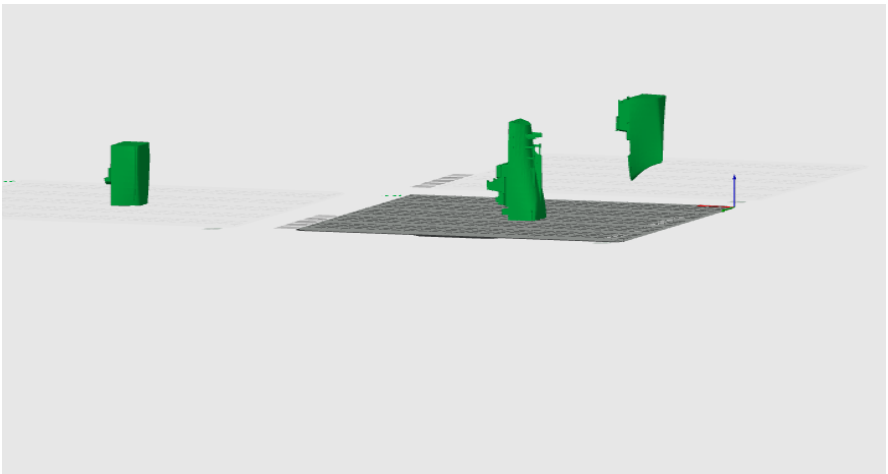

Figure. 13. θ **=90°**

After configuring the tilt angle as depicted in Fig. 13, the support mass and printing time for each part of the model are presented in the subsequent Table. The variation in printing time compared to the unsupported model is detailed in Table 9 below:

Table 9. Support mass, forming time and time difference.

Model parts	Support mass	Printing time	Time difference
A	2.51 g	87 min	35 min
B	0.74 g	46 min	15 min
C	4.86 g	68 min	32 min

The cumulative printing time for the three sections amounts to 219 minutes, with a combined support mass of 8.11g. In contrast, the original model tilted at a 90-degree angle requires 207 minutes of printing time, with a support mass totaling 15.99g. While the data confirms that the printing time for the sections remains greater than that for the entire model, the support required is nearly halved.

5.4.2 Set the Tilt Angle of Part A，Part B and Part C θ = -90°

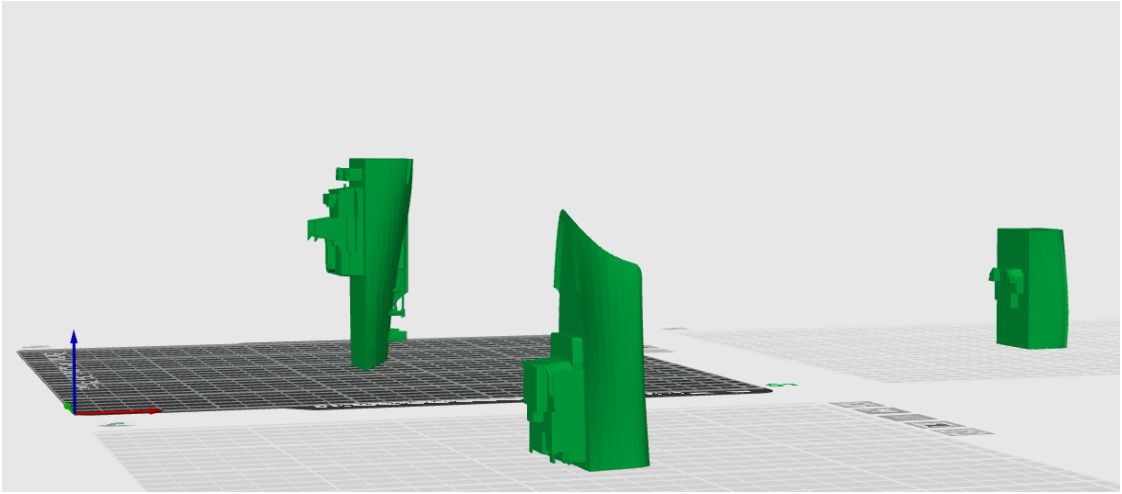

Figure. 14. Cross-section locate on the print plate

Printing time, support mass and other data are shown in the Table 10 below:

Table 10. θ = -90°.

Model parts	Support mass	Printing time	Time difference
A	6.01 g	93 min	41min
B	1.12 g	47 min	16 min
C	1.79 g	63 min	27 min

When compared to θ=90°, part A exhibited a nearly 50% reduction in contact area with the print tray, an impressive 139.44% surge in support mass, and a 17.14% augmentation in printing time. On the other hand, part B showed a marginal increase in contact area, accompanied by a 54% enhancement in support mass and a modest 6.06% rise in printing time. In contrast, part C displayed a significant augmentation in contact area with the print

tray, but experienced a 63.16% decrement in support mass and a noteworthy 15.62% reduction in printing time. In essence, the model's contact area with the print tray exhibits noTable variations, which correlate significantly with both printing time and support mass. Specifically, as the contact area enlarges, the support mass tends to diminish, while the print time shortens.

6. UV-curing 3D printing

The sliced layer thickness is set to 0.2 mm per layer, consistent with that of an FDM printer, while the resin density is established at 1.1 g/ml. Despite selecting a deflated model with a deflation coefficient of K=1\800 as the focal point of our study, the deflated models encompass the original model, Model A, Model B, and Model C. Initially, the deflated original model is employed to explore the interplay between tilt angle, support mass, and printing duration. The method to vary support is achieved by adjusting the model's placement angle. Tilt angles θ = [0°, 10°, 12°, 15°, 18°, 20°, 25°, 28°, 30°, 35°, 45°, 60°, 75°, 80°, 90°] are selected for examination. This research delves into 3D printing technology.

6.1 Relevant data from the original model

When θ = 0, the model's mass measures 121.3g. Support adjustments are made by altering the placement angle, and the corresponding printing times for different support configurations are recorded. Specific data are detailed in Table 11 below:

Table 11. In light curing, the relationship between tilt angle and support mass, forming time.

θ	Support mass (g)	Forming time (min)
0	0	47
10	28.7	79
12	29.9	84
15	33.7	92
18	36.6	99
20	39.1	104
25	41.6	121
28	42.5	131
30	41	137
35	44.6	152
45	42	178
60	26.7	212
75	26.5	236
80	25.1	241
90	38.9	245

6.1.1 Create a Line Graph Illustrating the Relationship Between Tilt angle, Print Time And Support Mass

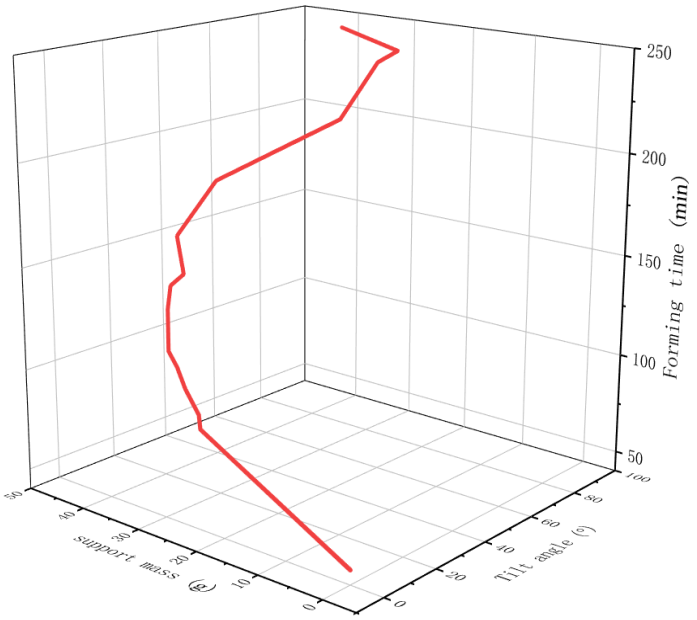

Figure. 15. Diagram depicting the relationship between the three variables.

Observing the 3D plot, a discernible positive correlation among the three variables becomes apparent. Specifically, within the range of θ-values from 0° to 20°, the curve exhibits a gradual incline. As the θ-value extends to the range of 0° to 60°, the curve steepens noticeably. Further, as the θ-value progresses beyond 60° to 80°, the curve's incline moderates, yet maintains a relatively swift growth rate. However, beyond this range, the curve flattens considerably, nearly stabilizing.

6.2 Segmented Printing in Light Curing

Set the tilt angle to θ=0°, import the deflated models of parts A, B, and C without support mass and forming time data for each part are presented in the Table 12 below:

Table 12. Modelling mass and forming time.

Model	Model mass	Forming time
A	50.7 g	47 min
B	39 g	35 min
C	31.5 g	43 min

The combined mass of the three parts amounts to 121.2g, which is 0.1g less than the original model. Additionally, the combined forming time for these parts totals 145 minutes, marking an increase of 98 minutes compared to the original model, approximately 208% longer. By consolidating the segmented printing data, it becomes evident that while the total mass of all segmented models remains relatively similar to that of the original model, there's a significant increase in forming time.

6.3 Separate Printing (FDM)

The data in part A are shown in the Figure16 and Table 13 below:

Table 13. Data Tables for part A.

θ (°)	**Support mass (g)**	**Printing time (min)**
0	0	47
10	4.8	60
12	4.7	61
15	4.7	62
18	4.8	64
20	4.9	65
25	4.3	73
28	4.1	77
30	4	79
35	3.7	85
45	4	96
60	2.6	107
75	1.9	111
80	2.3	111
90	1.8	108

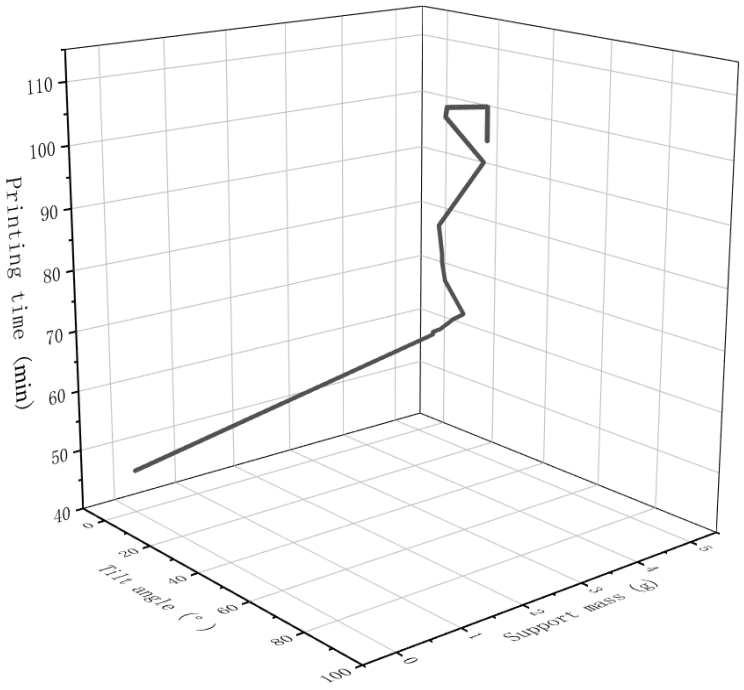

Figure. 16. Line graph of the three relationships in part A

The data in part B are shown in the Figure17 and Table 14 below:

Table 14. Data Tables for part B.

θ (°)	Support mass (g)	Printing time (min)
0	0	35
10	3.7	45
12	3.6	46
15	3.7	48
18	3.8	51
20	3.4	53
25	3.4	57
28	3	59
30	3.1	60
35	3	64
45	2.3	69
60	0.3	74
75	0.5	75
80	0.5	74
90	0.6	71

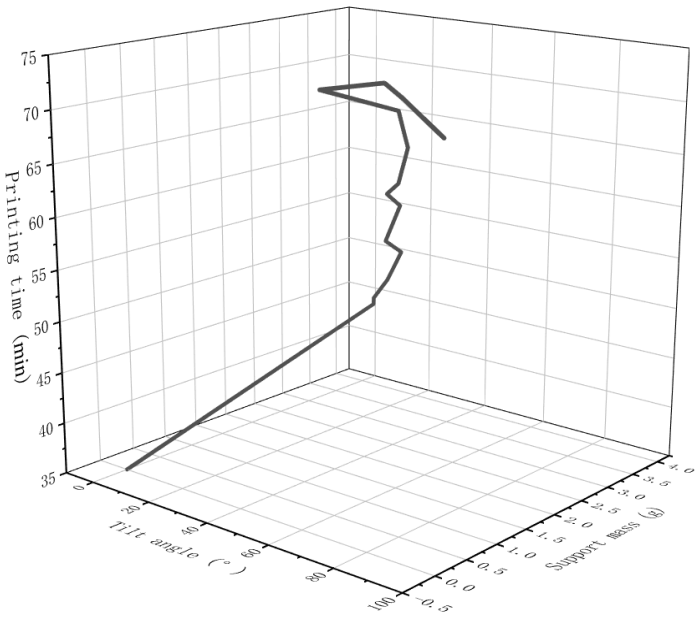

Figure. 17. Line graph of the three relationships in part B

The data in part C are shown in the Figure18 and Table 15 below:

Table 15. Data Tables for part C.

θ (°)	Support mass (g)	Printing time (min)
0	0	43
10	3.1	56
12	3.5	57

15	2.6	59
18	2.6	62
20	2.7	64
25	2.1	67
28	2.3	69
30	2.4	70
35	2.4	73
45	1.9	78
60	1.8	85
75	1.4	93
80	1.3	94
90	1.6	95

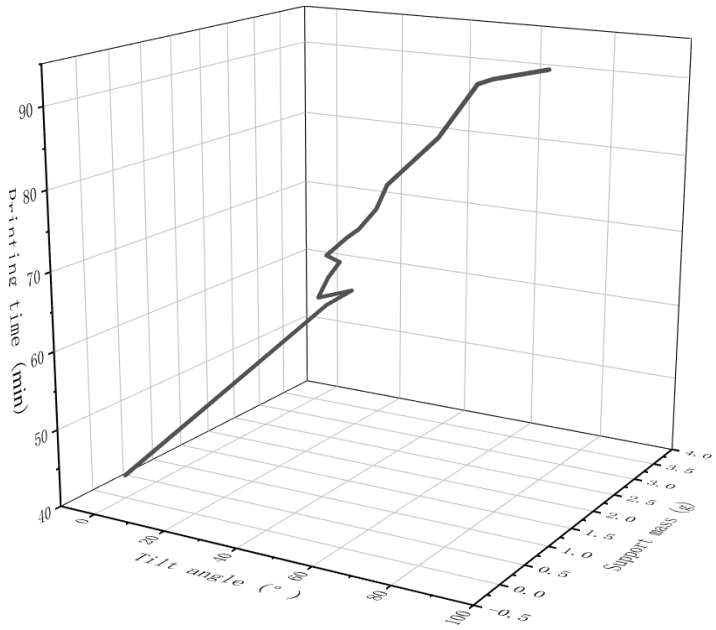

Figure. 18. Line graph of the three relationships in part C

Upon comparing Fig. 15 to Fig. 18, it becomes evident that the four fold lines exhibit a remarkably similar trend of change. Specifically, during the segmental printing process, all three segments of the fold lines display a steep upward trend at θ = 20°. At this juncture, the support mass remains within a narrow fluctuating range as the inclination angle gradually increases. Conversely, printing time exhibits a consistent upward trajectory. As the fold line begins to flatten around θ = 60°, the support mass diminishes with further tilt angle increment, while printing time continues to steadily rise.

Shifting our attention to the variable of tilt angle, it becomes apparent that support mass and molding time do not exhibit clear regularity when the tilt angle is constant. However, when support mass remains consistent, there is a clear positive correlation with printing time. Taking a broader perspective, a stronger correlation emerges between tilt angle and printing time. We also know from these data that the sum of the support masses required for

segmented printing is less than the sum of the masses when not segmented, but printing is the opposite.

7. Conclusions and Recommendations

Based on the experimental data from the two additive manufacturing processes, it's observed that the mass of the support increases as the tilt angle of the model placement varies from 0 to 40 degrees. Beyond 40 degrees, however, the mass begins to decrease initially before rising again. There appears to be no discernible correlation between the support mass and the forming time of the model. In FDM 3D printers, a localized pattern emerges between the tilt angle and forming time, whereas in light-curing 3D printers, the placement angle directly correlates with forming time

When employing both processes for segmented printing, the combined masses of each segment show no significant difference compared to the original unsegmented model. However, there is a significant increase in the forming time of the model. To ensure shorter modeling times and minimize material consumption, the following three recommendations are proposed:

1. Maximize the model within each segment; in other words, reduce the segmentation of the model.
2. The contact area between the model and the printing plate is as large as possible
3. Keep the distance between the print plate and the model's highest point as minimal as possible
4. Avoiding material concentration in 3D printing affects the surface quality of the model.

The inclination angle $\theta = 0^\circ$ of the model in this experiment adheres to the aforementioned three suggestions, effectively minimizing both molding time and support mass. However, excessive material concentration can result in suboptimal texture or even missing details, compounded by the "staircase effect" [28]. In such cases, it becomes necessary to adjust the model's placement angle accordingly. Having accurate data on all aspects of manufacturing a part can be very useful in saving costs and time, for example, offshore facilities vary in size and shape and each offshore facility requires specific design and testing [29]. For further insights into the structural integrity of the final print and guidance on designing segmented print structures effectively, readers can explore resources on ship structural strength design [30,31] or consult a local expert in the field.

Acknowledgments: I am very sincerely grateful to Dr. Dapeng Zhang for his guidance and direction of my research; I am also grateful to Yi Zhang and Yining Zhang for pointing out the errors in my article and guiding the revision so that we can have a higher quality article, and I am also grateful to Yifan Xie for his help with the technique and instrumentation; I am very grateful to the various people for their help!

Funding: This work was financially supported by Program for Scientific Research Start-up Funds of Guangdong Ocean University (grant number 060302112008) and the National Natural Science Foundation of China (grant number 62272109) .

Conflict of interest: The authors of the article have consulted with each other and have no conflict of interest.

References:

1. Bikas, Harry, Panagiotis Stavropoulos, and George Chryssolouris. "Additive manufacturing methods and modelling approaches: a critical review." The International Journal of Advanced Manufacturing Technology. 2016; 83: 389-405.
2. Dilberoglu, Ugur M., et al. "The role of additive manufacturing in the era of industry 4.0." Procedia manufacturing. 2017; 11: 545-554.
3. Li, Mengzhen, C. Guedes Soares, and Renjun Yan. "Free vibration analysis of FGM plates on Winkler/Pasternak/Kerr foundation by using a simple quasi-3D HSDT." Composite Structures. 2021; 264: 113643.
4. Qiu, Yu, et al. "An improved numerical method for calculating mechanical properties of bi-modulus sandwich composite structures." Ocean Engineering. 2022; 250: 110998.
5. Zhang, Yi, Dapeng Zhang, and Haoyu Jiang. "A review of artificial intelligence-based optimization applications in traditional active maritime collision avoidance." Sustainability. 2023;15.18: 13384.
6. Meng Ling adolescent. On the application of 3D printing in the field of shipbuilding[J]. China Equipment Engineering. 2020(07): 193-194.(in Chinese)
7. Liang Z., Si K., Xie Y., Lin Q., Zhao G., Zhang Y. A Study of Small-Scale Aircraft Carrier Modelling in Educational Practice. Eng. Solut. Mech. Mar. Struct. Infrastruct., 2024, 1(2).
8. MEI Menglei,QIN Qi,FANG Xinyue,et al. Introduction to the application of 3D printing technology in the field of ships[J]. Guangdong Shipbuilding,2023,42(06):70-72+77.(in Chinese)
9. Chang, Kuang-Hua. Motion Simulation and Mechanism Design with SOLIDWORKS Motion 2024. SDC publications, 2024.
10. Bethune, James D. Engineering Design and Graphics with SolidWorks 2019. Macromedia Press, 2019.
11. Mamajonova, Nodira, et al. "Exploring the Possibilities of 3DS MAX in Architectural Design: A Comprehensive Review." HOLDERS OF REASON 2.1 (2024): 383-391.
12. Patil, Sonali, Yogesh Deshpande, and Dattatraya Parle. "Extracting Slicer Parameters from STL file in 3D Printing." International Journal of Intelligent Systems and Applications in Engineering. 2024; 12.14s: 192-204.
13. Lee, Ching Hao, et al. "Potential for natural fiber reinforcement in PLA polymer filaments for fused deposition modeling (FDM) additive manufacturing: A review." Polymers 2021; 13.9: 1407.

14. Awasthi, Pratiksha, and Shib Shankar Banerjee. "Fused deposition modeling of thermoplastic elastomeric materials: Challenges and opportunities." Additive Manufacturing. 2021; 46: 102177.
15. Shichong, W. A. N. G., et al. "Development and applications of UV-curing 3D printing and photosensitive resin." Journal of Functional Polymers. 2022; 35.1: 19-35.
16. Kim, Ye Chan, et al. "UV-curing kinetics and performance development of in situ curable 3D printing materials." European Polymer Journal. 2017; 93: 140-147.
17. Wang Shichong,Zhu Yuwei,Wu Yao,et al. Development and application of light-curing 3D printing technology and photosensitive resin[J]. Journal of Functional Polymers. 2022; 35(01): 19-35.(in Chinese)
18. Dogan, Mustafa Doga, et al. "G-ID: identifying 3D prints using slicing parameters." Proceedings of the 2020 CHI Conference on Human Factors in Computing Systems. 2020.
19. Zhang, Yi, Dapeng Zhang, and Haoyu Jiang. "Review of Challenges and Opportunities in Turbulence Modeling: A Comparative Analysis of Data-Driven Machine Learning Approaches." Journal of Marine Science and Engineering. 2023; 11.7: 1440.
20. Zhang Y., Xie Y., Zhao G., Liang Z., Shi J., Yang Y. The Important Role of Fluid Mechanics in the Engineering Field. Eng. Solut. Mech. Mar. Struct. Infrastruct. 2024; 1(2).
21. Zhang, D., Zhao, B., Zhang, Y., and Zhou, N. "Numerical simulation of hydrodynamics of ocean-observation-used remotely operated vehicle." Frontiers in Marine Science. 2024; 11: 1357144.
22. Cao Yali.Research on the accuracy of 3D printing slicing software[J]. Screen Printing. 2023(14):91-93. (in Chinese)
23. Zhang, Duan Zhong, Jiajia Waters, and Paul Linford Barclay. Material point generation from an STL file. No. LA-UR-22-30587. Los Alamos National Laboratory (LANL), Los Alamos, NM (United States), 2022.
24. Kumar, Ajay, et al. "Printing file formats for additive manufacturing technologies." Advances in Additive Manufacturing. 2023: 87-102.
25. Wüthrich, Michael, et al. "A novel slicing strategy to print overhangs without support material."Applied Sciences. 2021; 11.18: 8760.
26. Tricard, Thibault, Frédéric Claux, and Sylvain Lefebvre. "Ribbed support vaults for 3D printing of hollowed objects." Computer Graphics Forum. Vol. 39. No. 1. 2020.
27. Singh, Jatinder, et al. "Influence of process parameters on mechanical strength, build time, and material consumption of 3D printed polylactic acid parts." Polymer Composites. 2022; 43.9: 5908-5928.

28. Haidiezul, A. H. M., A. F. Aiman, and B. Bakar. "Surface finish effects using coating method on 3D printing (FDM) parts." IOP Conference Series: Materials Science and Engineering. Vol. 318. IOP Publishing, 2018.
29. Zhang, Yi, Dapeng Zhang, and Haoyu Jiang. "A review of artificial intelligence-based optimization applications in traditional active maritime collision avoidance." Sustainability. 2023; 15.18: 13384.
30. Chen, Diyi, et al. "Research on Structural Strength of Different Car Ro-Ro Ships by Comparison Between Flexible and Rigid Deck Designs in Upright Condition." *ISOPE International Ocean and Polar Engineering Conference*. ISOPE, 2018.
31. Chen, Diyi, et al. "Research on Structural Strength of Different Car Ro-Ro Ships by Comparison Between Flexible and Rigid Deck Designs in Upright Condition." *ISOPE International Ocean and Polar Engineering Conference*. ISOPE, 2018.